Multidisciplinary | Rapid Review | Open Access Journal

A Rapid and Accurate Technique with Updating Strategy for Surface Defect Inspection of Pipelines

Y. Da[1], B. Wang[1], D. Liu[2], Z. Qian[1]

[1]State Key Laboratory of Mechanics and Control of Mechanical Structures, College of Aerospace Engineering, Nanjing University of Aeronautics and Astronautics, Nanjing, China
[2]School of Engineering, University of East Anglia, Norwich NR4 7TJ, UK

Corresponding authors: D. Liu (dianzi.liu@uea.ac.uk); Z. Qian (qianzh@nuaa.edu.cn).

This work was supported in part by the State Key Laboratory of Mechanics and Control of Mechanical Structures at NUAA under Grant MCMS-E-0520K02, in part by the Key Laboratory of impact and Safety Engineering, Ministry of Education, Ningbo University under Grant CJ201904, in part by the National Natural Science Foundation of China under Grant 11502108, 1611530686.

ABSTRACT Defect inspection in pipes at the early stage is of crucial importance to maintain the ongoing safety and suitability of the equipment before it presents an unacceptable risk. Due to the nature of detection methods being costly or complex, the efficiency and accuracy of results obtained hardly meet the requirements from industries. To explore a rapid and accurate technique for surface defects detection, a novel approach QDFT (Quantitative Detection of Fourier Transform) has been recently proposed by authors to efficiently reconstruct defects. However, the accuracy of this approach needs to be further improved. In this paper, a modified QDFT method with integration of an integral coefficient updating strategy, called as QDFTU, is developed to reconstruct the defect profile with a high level of accuracy throughout iterative calculations of integral coefficients from the reference model updated by a termination criteria (RMSE, root mean square error). Moreover, dispersion equations of circumferential guided waves in pipes are derived in the helical coordinate to accommodate the stress and displacement calculations in the scattered field using hybrid FEM. To demonstrate the superiority of the developed QDFTU in terms of accuracy and efficiency, four types of defect profiles, i.e., a rectangular flaw, a multi-step flaw, a double-rectangular flaw, and a triple-rectangular flaw, are examined. Results show the fast convergence of QDFTU can be identified by no more than three updates for each case and its high accuracy is observed by a smallest difference between the predicted defect profile and the real one in terms of mean absolute percentage error (MSPE) value, which is 6.69% in the rectangular-flaw detection example.

INDEX TERMS Circumferential guided wave, Hybrid FEM, Reconstruction, Reference model, Updating strategy

I. INTRODUCTION

Defects have a significant impact on the product quality and load-carrying capacity of structures and directly deteriorate effective material properties, which will lead to structural failure[1-3]. Therefore, defect detection is a key step to maintain structures with a long service life and has been paid more attentions in recent years. As one of the main detection techniques, ultrasonic guided waves have been widely used to detect defection in structures by many researchers (for example, Leonard et al.[4]; Huthwaite[5,6]; Jing et al.[7]; Hosoya et al.[8]). To comply with the enhanced inspection requirements, research on improving the accuracy and reliability of inspection has become necessary. Damage imaging is one of the approaches available for damage inspection, and a sub-branch of this approach is image reconstruction. The traditional image

reconstruction method is applied in the areas of optics and acoustics to solve wave-field reconstruction problems. However, the results obtained are not very satisfactory due to its single reconstruction mechanism. Therefore, iterative reconstruction methods have been proposed to improve the quality of the reconstruction results in optical fields[9-13]. In order to obtain the reconstruction results with a high level of accuracy, the forward problem has to be solved repeatedly. Since the computational time required to find the solution to forward problems is expensive, this reduces the efficiency and the ease of use of the iterative reconstruction methods. To overcome these limitations, many researchers have contributed their efforts to develop fast iterative methods. Sauer and Boouman[14] presented a local updater strategy for iterative reconstructions, which can enhance the reconstruction efficiency depending on updates of single pixel values rather than the entire image. Wang et al.[15] investigated and implemented two iterative image reconstruction methods in three dimensional optoacoustic tomography. With the availability of more powerful computing capacities, a model-based iterative reconstruction algorithm implemented on a modern graphics adapter (GPU) was proposed by Beister et al.[16].

Recently, the iterative technique has also been applied to the defect reconstruction using guided wave tomography. Huthwaite and Simonetti[17] extended HARBUT (the Hybrid Algorithm for Robust Breast Ultrasound Tomography) to generate thickness maps for guided wave tomography, and used the iterative HARBUT to improve the accuracy of reconstructions of defects. Yang et al.[18] developed an iterative S-wave velocity inversion method guided by image registration. Rao et al.[19] proposed a guided wave tomography method based on full waveform inversion (FWI), which was iteratively applied to discrete the frequency components from low to high frequencies.

Defect reconstruction based on the boundary integral equation (BIE) of ultrasonic waves is an effective quantitative detection approach[20-22] in the field of non-destructive testing. In this method, most of defects are approximately reconstructed using simplified total fields, which are normally obtained by Born approximation, Rytov approximation and Kirchhoff approximation[23-27]. However, these approximate reconstructions cannot be improved by iteration method due to the failure of updating total fields in the defected structures. Recently, QDFT (Quantitative Detection of Fourier Transform) proposed by authors[28] has overcome this disadvantage and shed light on the application of iterative methods for reconstruction of defects.

It is well known that the guided waves can be employed to detect defects in plate-like or bending structures. The applications of guided waves were described in non-cylindrical structures [29-33], such as railway rails and structural 'I' beams. Liu et al.[34] proposed a method to detect radial cracks in annular structures and its methodology built on guided circumferential waves and continuous wavelet transform. Sanderson et al.[35] adopted finite element analysis and experiments to explain the received signal changes caused by the pipe bending. Leinov et al.[36] investigated the propagation and attenuation of guided waves in pipe buried in sand. Based on the existing investigations of circumferential guided waves[37-44], it is necessary to derive the general dispersion equations of circumferential guided waves using an equidistant surface coordinate so that the stress and displacement calculations can be easily accommodated in the scattered field. There are mainly two difficulties for the defect detection on pipelines. The numerical simulation of circumferential scattered waves is studied. And the analytical fundamental solution in pipelines, which is often used to build the mapping relationship between the defect function and the signal of scattered waves, is hardly found.

In this paper, a modified QDFT (Quantitative Detection of Fourier Transform) method with integration of an integral coefficient updating strategy, called the QDFTU, is proposed to reconstruct the defect profile. QDFT is a quantitative reconstruction method based on the reference model, which demonstrates that the defect profile in the two dimensional problem can be formulated as an inverse Fourier transform of the product of reflected coefficients from the detected structure and integral coefficients from the reference model, where the referred defect can be arbitrarily selected. The research mainly contains two parts of forward problems and inverse problems. For forward problems, a semi-analytical FEM is applied to solve the dispersion equations of circumferential guided waves, which are derived in the equidistant surface coordinate. Then, the scattered fields in a circular annulus are calculated using the developed hybrid FEM technique. To reconstruct defects in the phase of inverse problems, the proposed QDFTU is applied to reconstruction defects with high levels of accuracy and efficiency throughout iterative calculations of integral coefficients from the updated reference model, where the termination is controlled by a convergence criterion. Finally, its correctness has been verified by four numerical examples.

II. DISPERSION EQUATIONS OF CIRCUMFERENTIAL GUIDED WAVES AND CALCULATION OF SCATTERED FIELDS

The analysis of guided wave dispersion is of great importance to grasp the propagation mechanism in the structure. It can help to select effective modes of guided waves in the calculation of scattered fields caused by defects. In this paper, our aim is the detection of surface defect in the cross section of hollow cylinder (i.e. circular annulus). Therefore, the circumferential guided waves are mainly focused. Even so, we try to solve this problem in the 3D curved coordinate system $(\alpha_1, \alpha_2, \alpha_3)$ as shown in Fig.1.

And an improved semi-analytical finite element method (SAFEM) is introduced to deal with it. Taking into account this coordinate system, various helical guided waves must exist due to different incident angle φ of guided waves. Therefore, this model in the curved coordinate system $(\alpha_1,\alpha_2,\alpha_3)$ is more universal for studying possible guided waves in a hollow cylinder. In this opinion, for the circumferential guided waves that is particularly concerned, they can be viewed as a special case from the helical guided waves as $\varphi=0$. Consequently, generalized helical guided waves are firstly analyzed by the improved SAFEM, and then the result of circumferential guided waves can be extracted from the solution of helical guided waves. For helical guided waves propagating with an arbitrary angle in a hollow cylinder, the curvatures for the geodesics[45], which are spirals on the surface of the hollow cylinder, can be expressed

$$k_1^{\varphi}=\kappa_1\cos^2\varphi+\kappa_2\sin^2\varphi,\quad k_2^{\varphi}=\kappa_1\sin^2\varphi+\kappa_2\cos^2\varphi \tag{1}$$

where $\kappa_1=1/r_{\text{out}}$ and $\kappa_2=0$, which are the principal curvatures of the outside surface with the radius r_{out} in a cylindrical system. The curvatures of the generalized coordinate α_1 and α_2 are denoted as k_1^{φ} and k_2^{φ}, respectively. Hence, Lame coefficients[45] (scale factors) can be written as follows

$$h_1=1+k_1^{\varphi}\alpha_3\ ,\ h_2=1+k_2^{\varphi}\alpha_3\ ,\ h_3=1 \tag{2}$$

where the outsider surface is considered as the reference surface of equidistant surface.

Thus, the relationships between the particle displacements u_i and strains ε_{ij} are represented as

$$\begin{aligned}
\varepsilon_{11}&=\frac{1}{h_1}\frac{\partial u_1}{\partial\alpha_1}+\frac{k_1^{\varphi}}{h_1}u_3,\\
\varepsilon_{22}&=\frac{1}{h_2}\frac{\partial u_2}{\partial\alpha_2}+\frac{k_2^{\varphi}}{h_2}u_3,\ \varepsilon_{12}=\frac{1}{2}\left(\frac{1}{h_1}\frac{\partial u_2}{\partial\alpha_1}+\frac{1}{h_2}\frac{\partial u_1}{\partial\alpha_2}\right),\\
\varepsilon_{33}&=\frac{\partial u_3}{\partial\alpha_3},\\
\varepsilon_{13}&=\frac{1}{2}\left(\frac{1}{h_1}\frac{\partial u_3}{\partial\alpha_1}+\frac{\partial u_1}{\partial\alpha_3}-\frac{k_1^{\varphi}}{h_1}u_1\right),\\
\varepsilon_{23}&=\frac{1}{2}\left(\frac{1}{h_2}\frac{\partial u_3}{\partial\alpha_2}+\frac{\partial u_2}{\partial\alpha_3}-\frac{k_2^{\varphi}}{h_2}u_2\right)
\end{aligned} \tag{3}$$

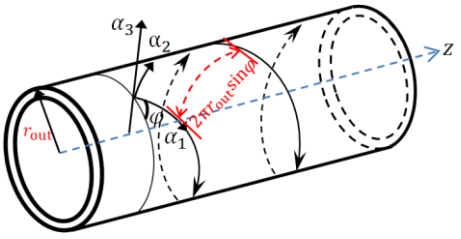

FIGURE 1. Helical guided waves propagating along α_1 direction in a pipe. r_{out} represents the outer radius of a pipe, the range of α_2 is $[0,2\pi r_{\text{out}}\sin\varphi)$, and φ denotes the incident angle defined by the axis α_1 and the circumferential direction of the pipe.

Rewriting (3) in a matrix form, one has

$$\boldsymbol{\varepsilon}=\begin{bmatrix}
\frac{1}{h_1}\frac{\partial}{\partial\alpha_1} & 0 & \frac{k_1^{\varphi}}{h_1}\\
0 & \frac{1}{h_2}\frac{\partial}{\partial\alpha_2} & \frac{k_2^{\varphi}}{h_2}\\
0 & 0 & \frac{\partial}{\partial\alpha_3}\\
0 & \frac{\partial}{\partial\alpha_3}-\frac{k_2^{\varphi}}{h_2} & \frac{1}{h_2}\frac{\partial}{\partial\alpha_2}\\
\frac{\partial}{\partial\alpha_3}-\frac{k_1^{\varphi}}{h_1} & 0 & \frac{1}{h_1}\frac{\partial}{\partial\alpha_1}\\
\frac{1}{h_2}\frac{\partial}{\partial\alpha_2} & \frac{1}{h_1}\frac{\partial}{\partial\alpha_1} & 0
\end{bmatrix}\begin{bmatrix}u_1\\u_2\\u_3\end{bmatrix}=\mathbf{L}\mathbf{u} \tag{4}$$

The partial derivative $\frac{\partial}{\partial\alpha_i}$, where $i=1,2,3$, expresses displacement derivative along the axis α_i, and

$$\mathbf{L}=\mathbf{L}_1\frac{1}{h_1}\frac{\partial}{\partial\alpha_1}+\mathbf{L}_2\frac{1}{h_2}\frac{\partial}{\partial\alpha_2}+\mathbf{L}_3\frac{\partial}{\partial\alpha_3}+\mathbf{L}_4\frac{k_1^{\varphi}}{h_1}+\mathbf{L}_5\frac{k_2^{\varphi}}{h_2},$$

$$\mathbf{L}_1=\begin{bmatrix}1&0&0\\0&0&0\\0&0&0\\0&0&0\\0&0&1\\0&1&0\end{bmatrix},\mathbf{L}_2=\begin{bmatrix}0&0&0\\0&1&0\\0&0&0\\0&0&1\\0&0&0\\1&0&0\end{bmatrix},\mathbf{L}_3=\begin{bmatrix}0&0&0\\0&0&0\\0&0&1\\0&1&0\\1&0&0\\0&0&0\end{bmatrix},$$

$$\mathbf{L}_4=\begin{bmatrix}0&0&1\\0&0&0\\0&0&0\\0&0&0\\-1&0&0\\0&0&0\end{bmatrix},\mathbf{L}_5=\begin{bmatrix}0&0&0\\0&0&1\\0&0&0\\0&-1&0\\0&0&0\\0&0&0\end{bmatrix} \tag{5}$$

Discretizing the hollow cylinder along the wall thickness direction (α_3), the displacements are represented as:

$$\mathbf{u}(\alpha_1,\alpha_2,\alpha_3)=\begin{bmatrix}u_1&u_2&u_3\end{bmatrix}^T=\mathbf{N}(\alpha_3)\boldsymbol{U}(\alpha_1,\alpha_2) \tag{6}$$

where $\mathbf{N}$ is a matrix of shape functions of an element.

The relationship between strains and displacements can be obtained by substituting (5) and (6) into (4),

$$\begin{aligned}
\boldsymbol{\varepsilon}=\mathbf{L}\mathbf{u}&=\mathbf{L}_1\frac{1}{h_1}\mathbf{N}\boldsymbol{U}_{,1}+\mathbf{L}_2\frac{1}{h_2}\mathbf{N}\boldsymbol{U}_{,2}\\
&+\mathbf{L}_3\mathbf{N}_{,3}\boldsymbol{U}+\mathbf{L}_4\frac{k_1^{\varphi}}{h_1}\mathbf{N}\boldsymbol{U}+\mathbf{L}_5\frac{k_2^{\varphi}}{h_2}\mathbf{N}\boldsymbol{U}
\end{aligned} \tag{7}$$

It is noted that the mapping relationship between the helical coordinate system and cylindrical coordinate system implies the effective interval of the axis α_2 in Fig. 1, which is in the range of $\left[0, 2\pi r_{\text{out}}\sin\varphi\right)$ except $\varphi = 0$, and the variable α_1. In order to formulate the displacement along the axis α_2, the periodic extension in which the defined interval l equates $2\pi r_{\text{out}}\sin\varphi$ along the axis α_2 must be introduced to achieve Fourier series. Therefore, the expression of the displacement $U(\alpha_1, \alpha_2)$ can be written as

$$\boldsymbol{U}(\alpha_1,\alpha_2) = \sum_n \mathrm{e}^{\mathrm{i}n\frac{2\pi}{l}\alpha_2}\boldsymbol{U}_n(\alpha_1) = \sum_n \mathrm{e}^{\mathrm{i}\xi_n\alpha_2}\boldsymbol{U}_n(\alpha_1), \quad n = \mathrm{L}\ -2,-1,0,1,2,\mathrm{L} \tag{8}$$

where $\xi_n = n2\pi/l$, ξ_n represents a wavenumber, and $\mathrm{i} = \sqrt{-1}$. It is explained that the subscript n represents the order number of Fourier series.

It is noted that (8) can describe the displacement field for plane problems by setting $n = \xi_n = 0$. For the special case $\varphi = 0$, it represents that the guided waves propagate along the circumferential direction of the pipe shown in Fig. 1. This propagation of guided waves is mainly considered for defect detection in this paper.

Hamilton's principle[46] is used to establish the motion equation,

$$\int_V \left(\delta\mathbf{u}^{\mathrm{T}}\rho\ddot{\mathbf{u}} + \delta\boldsymbol{\varepsilon}^{\mathrm{T}}\boldsymbol{\sigma}\right)dV = \int_V \delta\mathbf{u}^{\mathrm{T}}\mathbf{P}dV \tag{9}$$

where ρ is material density, $\boldsymbol{\sigma}$ is stress tensor, $\ddot{\mathbf{u}}$ means the second time derivative of the displacement, $\mathbf{P}$ represents the external loads, V represents the structure volume, and δ denotes a variational symbol. Substituting (7) and (8) into (9), and applying inverse Fourier transform over the axis α_1, i.e., $\bar{U}_n(\xi_n) = \frac{1}{2\pi}\int U_n(\alpha_1)\mathrm{e}^{\mathrm{i}\xi_n\alpha_1}d\alpha_1$. The final equation is expressed in the term of the eigen equation

$$\left[\mathbf{A}(\xi_n\omega) - \xi_n\mathbf{B}(\xi_n\omega)\right]\boldsymbol{Q}_n = \boldsymbol{P}_n,$$
$$\mathbf{A} = \begin{bmatrix} \mathbf{0} & \mathbf{W}+\mathbf{M}_3 \\ \mathbf{W}+\mathbf{M}_3 & \mathbf{M}_2 \end{bmatrix}, \mathbf{B} = \begin{bmatrix} \mathbf{W}+\mathbf{M}_3 & \mathbf{0} \\ \mathbf{0} & -\mathbf{M}_1 \end{bmatrix} \tag{10}$$

where

$$\mathbf{M}_1 = \int \mathbf{B}_1^T\mathbf{D}\mathbf{B}_1 h_1 h_2 d\alpha_3,$$

$$\mathbf{M}_2 = \int \left[\mathrm{i}\mathbf{B}_3^T\mathbf{D}\mathbf{B}_1 - \mathrm{i}\mathbf{B}_1^T\mathbf{D}\mathbf{B}_3 + \alpha_3\xi_2\mathbf{B}_2^T\mathbf{D}\mathbf{B}_1 + \alpha_3\xi_2\mathbf{B}_1^T\mathbf{D}\mathbf{B}_2\right]h_1 h_2 d\alpha_3,$$

$$\mathbf{M}_3 = \int \left[\mathrm{i}\alpha_3\xi_2\mathbf{B}_3^T\mathbf{D}\mathbf{B}_2 - \mathrm{i}\alpha_3\xi_2\mathbf{B}_2^T\mathbf{D}\mathbf{B}_3 + (\alpha_3\xi_2)^2\mathbf{B}_2^T\mathbf{D}\mathbf{B}_2 + \mathbf{B}_3^T\mathbf{D}\mathbf{B}_3\right]h_1 h_2 d\alpha_3,$$

$$\mathbf{B}_1 = \mathbf{L}_1\frac{1}{h_1}\mathbf{N}, \mathbf{B}_2 = \mathbf{L}_2\frac{1}{h_2}\mathbf{N}, \mathbf{B}_3 = \mathbf{L}_3\mathbf{N}_{,3} + \mathbf{L}_4\frac{\xi_1}{h_1}\mathbf{N} + \mathbf{L}_5\frac{\xi_2}{h_2}\mathbf{N},$$
$$\mathbf{W} = \int\left(-\omega^2\rho\mathbf{N}^T\mathbf{N}\right)h_1 h_2 d\alpha_3,$$

$$\boldsymbol{Q}_n = \begin{bmatrix}\bar{\boldsymbol{U}}_n & \xi_n\bar{\boldsymbol{U}}_n\end{bmatrix}^T, \ \boldsymbol{P}_n = \begin{bmatrix}\mathbf{0} & \bar{\boldsymbol{F}}_n\end{bmatrix}^T \tag{11}$$

ω is the circular frequency; $\bar{\boldsymbol{U}}_n$ represents displacements in the wavenumber domain, which are obtained by inverse Fourier transform of $\boldsymbol{U}_n(\alpha_1)$ in (8); and $\bar{\boldsymbol{F}}_n$ is the loads in the wavenumber domain and its definition is the same as $\bar{\boldsymbol{U}}_n$; $\mathbf{D}$ represents a matrix of elastic moduli. In order to obtain the nontrivial solutions of the dispersion equations, the determinant of the matrix in (10) should be equal to zero as follows:

$$\left|\mathbf{A}(\xi_n\omega) - \xi_n\mathbf{B}(\xi_n\omega)\right| = 0 \tag{12}$$

Solving (12), the left eigenvectors $\boldsymbol{\phi}_{nm}^L$ and right eigenvectors $\boldsymbol{\phi}_{nm}^R$ are obtained as functions of different eigenvalues k_{nm} (wavenumber), in which the subscript m means the order number of guided wave modes and n represents the number of the order of Fourier expansion along the axis α_2 direction in (8). Combining with Zhuang's work[47], the displacement and stress formulas ($\boldsymbol{U}_n$ and $\boldsymbol{\sigma}_n$) are derived as, in which the Fourier transform of displacements and stresses and Cauchy's integral theorem are adopted,

$$\boldsymbol{U}_n = -\frac{\mathrm{i}}{2\pi}\frac{k_{nm}\left[\boldsymbol{\phi}_{nmu}^L\right]^{\mathrm{H}}\boldsymbol{P}_n}{B_{nm}}\boldsymbol{\phi}_{nmu}^R\mathrm{e}^{-\mathrm{i}k_{nm}(\alpha_1-\alpha_0)} = \boldsymbol{\Phi}_{nm}\mathrm{e}^{-\mathrm{i}k_{nm}(\alpha_1-\alpha_0)},$$

$$\boldsymbol{\sigma}_n = \left\{\mathbf{D}\left[\left(\mathbf{B}_1 + \mathrm{i}n\xi_2\mathbf{B}_2 - \mathrm{i}k_{nm}\mathbf{B}_3\right)\boldsymbol{\Phi}_{nm}\right]\right\}\mathrm{e}^{-\mathrm{i}k_{nm}(\alpha_1-\alpha_0)} = \mathbf{t}_n\mathrm{e}^{-\mathrm{i}k_{nm}(\alpha_1-\alpha_0)} \tag{13}$$

where α_0 is the position of load $\boldsymbol{P}_n$ in axis α_1. By numerically solving the dispersion equations of helical guided waves in pipes with material properties shown in TABLE I, characterization of the hollow cylinder using the frequency dependence of the wave phase velocity can be observed in Fig. 2. It is emphasized that all numerical examples in this paper are simulated with $n = 0$.

Then the circumferential guided waves can be solved following above equations by letting $\varphi = 0$, and the corresponding results described by blue points can be found in Fig. 2. Because of non-dispersion of the first anti-plane mode $\mathrm{SH}^{\mathrm{st}}$, it is chosen as the incident guided waves to detect flaws. With this understanding, calculations of the displacement and stress scatted fields can be correctly conducted by the hybrid FEM[28]. The hybrid FEM divides the integrity structure into two components. The

displacements and stresses in the component without defects are expressed by the results calculated in (13). And for the other component involving defects, the traditional FEM is adopted to simulate. At the interface of these components, the continuous conditions of displacement and traction are utilized.

It is noted that without lost of generality, the dispersion equations of guided waves propagating in arbitrary direction are derived in a helical coordinate system. However, the circumferential guided waves propagating along the direction $\varphi = 0$ are applied to solve all numerical examples in this work.

TABLE I
MATERIAL PROPERTIES OF THE PIPE MODEL

Density	Inner radius	Outer radius	Wall thickness	Lame constants
$(\rho, \mathrm{kg/m^3})$	$(r_{\mathrm{in}}, \mathrm{m})$	$(r_{\mathrm{out}}, \mathrm{m})$	$(\mathrm{h} = r_{\mathrm{out}} - r_{\mathrm{in}})$	$(\lambda \, and \, \mu, \mathrm{Pa})$
8.232×10^{3}	3.881×10^{-2}	4.440×10^{-2}	5.590×10^{-3}	1.089×10^{11}, 8.430×10^{10}

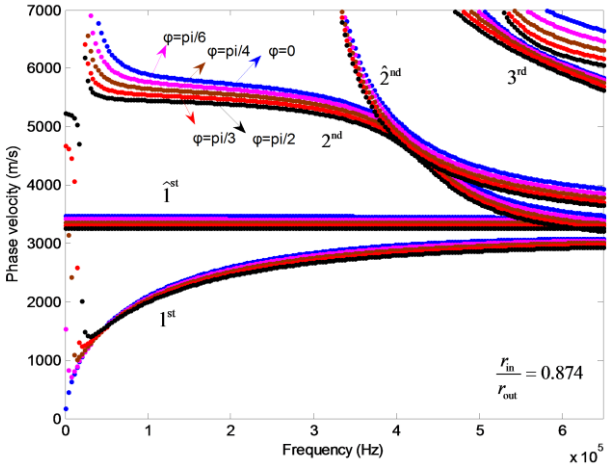

FIGURE 2. The dispersion curves of guided waves with difference incident angles ($\varphi = 0, \pi/6, \pi/4, \pi/3, \pi/2$ and ' ^ ' represents the anti-plane mode)

III. DEFECT RECONSTRUCTION APPROACH WITH AN INTEGRAL COEFFICIENT UPDATING STRATEGY

In following sections, the $\hat{1}^{st}$ circumferential guided wave calculated in Section 2 is adopted as the incident wave to detect 2D flaws in a circular annulus. QDFT proposed by Da et al.[28] is suitable for the detection of 2D structures. It demonstrates that the defect depth ($\eta(\alpha_1)$) depending on the propagation direction (α_1) of guided waves can be written as the Fourier transform of the product of reflection coefficients ($C^{\mathrm{ref}}(k)$) of guided waves and integral coefficients ($B_0(k)$) obtained from the reference model. When the incident angle φ is zero in Fig. 1, i.e., the current guided waves propagate along the circumferential direction, considering the 2D defect within cross section of hollow cylinder (i.e. circular annulus), the function $\eta(\alpha_1)$ of defect depth can be expressed as

$$\eta(\alpha_1) \approx \frac{1}{2\pi}\int_{-\infty}^{+\infty} C^{\mathrm{ref}}(k) B_0(k) \mathrm{e}^{\mathrm{i}k\alpha_1} dk \tag{14}$$

where $k = k_{nm}$ is the wavenumber of guided waves along the axial direction α_1 of the structure. In the following defect detection $n = 0$ and m represents the first anti-plane mode $\hat{1}^{st}$. $C^{\mathrm{ref}}(k)$ is the reflection coefficients of guided waves traveling in the tested structure, $B_0(k)$ represents the integral coefficient of the initial reference model, and $\eta(\alpha_1)$ denotes the profile of defects. Here, it is noted that the initial reference model can be chosen randomly, which was demonstrated in the previous paper[28].

However, the potential issue arising from this method is the accuracy of the predicted defect profiles. This is because the defect used in reference model cannot be selected as the same as the unknown flaw in inspected models, which leads to the discrepancy between the real defect and predicted one. To tackle this problem, a modified QDFT with the integration of an integral coefficient updating strategy (QDFTU) is proposed in this paper to reconstruct the defect profile with high levels of accuracy and efficiency throughout iterative calculations of integral coefficients from the reference model updated by a convergence criterion. Although an iteration method was successful applied in guided wave tomography[17,19], to the best of our knowledge, this is the first time to improve defect detection based on boundary integral equation (BIE). In QDFTU, the formula for defect reconstruction can be written as

$$\eta_i(\alpha_1) \approx \frac{1}{2\pi}\int_{-\infty}^{+\infty} C^{\mathrm{ref}}(k) B_{i-1}(k) \mathrm{e}^{\mathrm{i}k\alpha_1} dk, i = 1,2,3,\mathrm{L} \tag{15}$$

i represents the number of iteration reconstruction, B_{i-1} is the integral coefficient of the $(i-1)^{\mathrm{th}}$ reference model, and $\eta_i(\alpha_1)$ denotes the $(i)^{\mathrm{th}}$ reconstruction results.

The flowchart of QDFTU is shown in Fig. 3. The left block diagram provides an overview of defect detection, which mainly contains original data, scattering data, defect reconstruction, signal processing, and convergence verification. The original data are usually gained from testing or numerical simulation. The right diagram, which is the detailed description for the left one, includes two parts: a forward problem depicted in red box and an inverse problem described in purple box. Its methodology can be described as follows:

① Forward problem

Firstly, the selection of a simple reference model with one rectangular defect $\eta_i(\alpha_1)$ is suggested, and the

reflection coefficients $C^{\text{ref}}(k)$ of the tested circular annulus are calculated using hybrid FEM, which is used to replace the results from the experiment testing. Then, the defect profile $\eta_{i-1}(\alpha_1)$ of the reference model is converted into a defect function of $H_{i-1}(k)$ in the wavenumber domain by employing Fourier transform, where $H_{i-1}(k)=\int_{-\infty}^{+\infty}\eta_{i-1}(\alpha_1)\mathrm{e}^{ik\alpha_1}d\alpha_1$. Finally, the integral coefficients B_{i-1} of the reference model are obtained using the equation $B_{i-1}(k)=H_{i-1}(k)/C_{i-1}^{\text{ref}}(k)$. It is noted that the subscript 'i' represents the number of the updates by the reference model so that the defect profile obtained from reconstruction of defects described in the following section 'Inverse problem' converges.

② Inverse problem and the updating strategy

Based on our previous work, it is emphasized that the peak values of integral coefficients $B_{i-1}(k)$ must be modified when the reconstruction results show strong noise in non-defective region[28]. The modified integral coefficients $\tilde{B}_{i-1}(k)$ are used in the reconstructive formula $\eta_i(\alpha_1)\approx\frac{1}{2\pi}\int_{-\infty}^{+\infty}C^{\text{ref}}(k)\tilde{B}_{i-1}(k)\mathrm{e}^{ik\alpha_1}dk$ to obtain a new result. It is noted that $B_{i-1}(k)$ need not to be filtered when the noise in non-defect region is weak. Therefore, 'the signal processing **I**' described in the flowchart will be triggered only if the noise reaches a certain level of significance. To ensure the recognition of the defect's boundary and distinguish it from the whole inspected section, the values of $\eta_i(\alpha_1)$ in the non-defective zone are set to zeros in the phase of 'the signal processing **II**' due to the negligible noise. It is noted when the noise energy in non-defect zone is less than a quarter of the signal energy in defect zone, the noise is weak. Otherwise, it is considered as a strong noise signal.

In the process of defect reconstruction, the key problem is that how to estimate the correctness of the current reconstruction. Theoretically, a surface defect has unique reflection coefficients of guided waves and reconstruction of the defect should converge to the real defect, given the adequate resolution of guided waves. However, the reconstructed defect profile cannot be exactly the same as the real one. In this situation, to enhance the detection precision, a convergence criterion shown in (16) is used to evaluate the discrepancy between two consecutive reconstructions of defects.

$$\grave{o}=\sqrt{\frac{\sum_{m=1}^{N}\left[\left(\eta_i\left(\alpha_1^{(m)}\right)-\eta_{i-1}\left(\alpha_1^{(m)}\right)\right)^2\right]}{N}} \tag{16}$$

where N denotes the total sample number in the axis α_1, the subscript i indicates the number of reconstruction times, $\grave{o}$ means the root mean square error (RMSE), to which $\grave{o}_0$ is assigned as a threshold value in this paper. $\eta_i(\alpha_1)$, $\eta_{i-1}(\alpha_1)$, and $\eta_0(\alpha_1)$ denote the current, previous and reference defect profiles, respectively. If $\grave{o}\le\grave{o}_0$, the current result will be considered as the final profile. Otherwise, the current defect profile will replace the reference model and update the defect profile for the next iteration until the convergence criterion is satisfied. In this paper, the value $\grave{o}_0$ is identical to $0.1d_{\max}$, where $d_{\max}$ represents the largest depth of predicted defects."

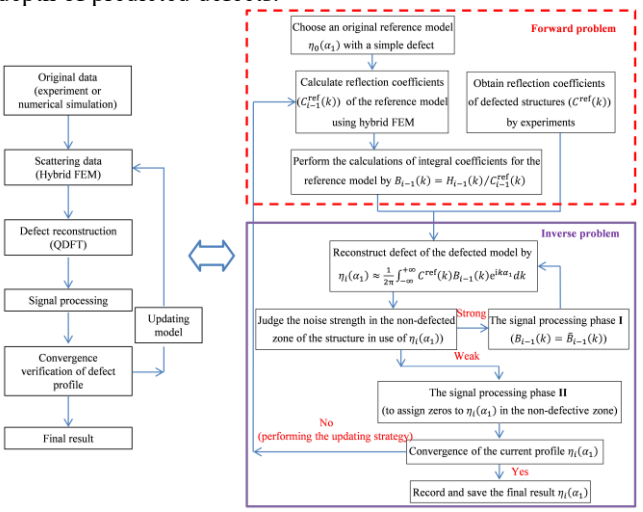

FIGURE 3. Flowchart of QDFTU method for surface defect reconstruction

VI. NUMERICAL EXAMPLES

A. RECTANGULAR FLAW

A representative example is examined in this section to demonstrate the capability of the proposed QDFTU approach to defect detection. Two simple annuli with different rectangular defects, a reference model shown in Fig. 4 and a predicted model in Fig. 5, are studied. By applying the hybrid FEM technique, reflection coefficients of guided waves in these two models have been calculated. It is noted that the frequency range of incident guided waves is from 6.159KHz to 683.702KHz, in which 112 equal frequency points are adopted to numerical simulation by the hybrid FEM in frequency domain. Defect reconstruction by QDFTU in the first iteration has been shown in Fig. 6(a), in which the integral coefficients $B_i(k)$ have been calculated using the reference model shown in Fig. 4. The data for construction of the defect profile can be obtained in the second column of TABLE Ⅱ. The first and last columns in TABLE Ⅱ represent the coordinates of the defect in the extent and radial directions. In the practical engineering testing, it is difficult to evaluate the defect profile using a single reconstruction owing to the unknown defect in structures. To improve the reliability of the

reconstruction, the proposed QDFTU approach works towards the converged defect profile. The first reconstruction result in Fig. 6(a) is adopted as the updated reference model in the second reconstruction, which is shown in Fig. 6(b) and the coordinate in the defect extent direction is given in the third column of TABLE Ⅱ. It is noted that the updating of the reference model terminates until the discrepancy ò is less than 0.03h, where $ò_0 = 0.030h$ and h means the thickness of the annulus. In TABLE Ⅱ, the discrepancies from the first and second reconstructions, i.e. $i = 2$, is equal to 0.080h, which is more than 0.030h. This is why the third reconstruction is triggered. Obviously, the third discrepancy (0.026h) between the second and third results is less than 0.030h and the result in the fourth column in TABLE Ⅱ is considered as the final defect profile. All defect profiles obtained from each reconstruction are shown in Fig. 6, which demonstrates the efficiency and effectiveness of the proposed QDTFU approach to reconstruction of defects.

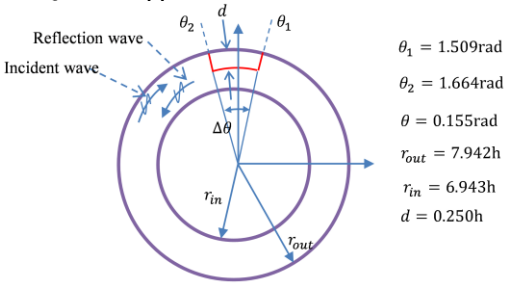

FIGURE 4. **The reference model with a single rectangular defect. The area enclosed by the red lines represents defect.**

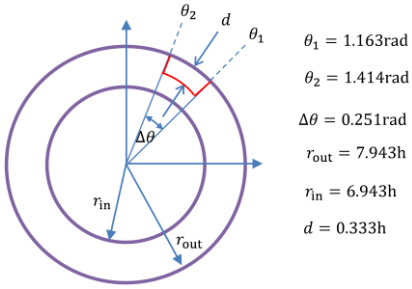

FIGURE 5. **The tested model with a single rectangular defect. The area enclosed by the red lines represents defect.**

TABLE Ⅱ
THE DATUM OF DEFECT SHAPE FROM THE ITERATIVE RECONSTRUCTION

Coordinate (rad)	Result (1^{st})*h	Result (2^{nd})*h	Result (3^{rd})*h	Real defect *h
1.158	0.068	0.086	0.108	0.333
1.187	0.124	0.218	0.211	0.333
1.215	0.181	0.328	0.296	0.333
1.243	0.239	0.368	0.334	0.333
1.271	0.291	0.352	0.315	0.333
1.299	0.328	0.316	0.290	0.333
1.328	0.343	0.314	0.306	0.333
1.356	0.333	0.353	0.343	0.333
1.384	0.294	0.381	0.350	0.333
1.413	0.226	0.339	0.307	0.333
1.441	0.144	0.211	0.214	0.333
1.469	0.065	0.064	0.10	0.333
ò		**0.080**	**0.026**	

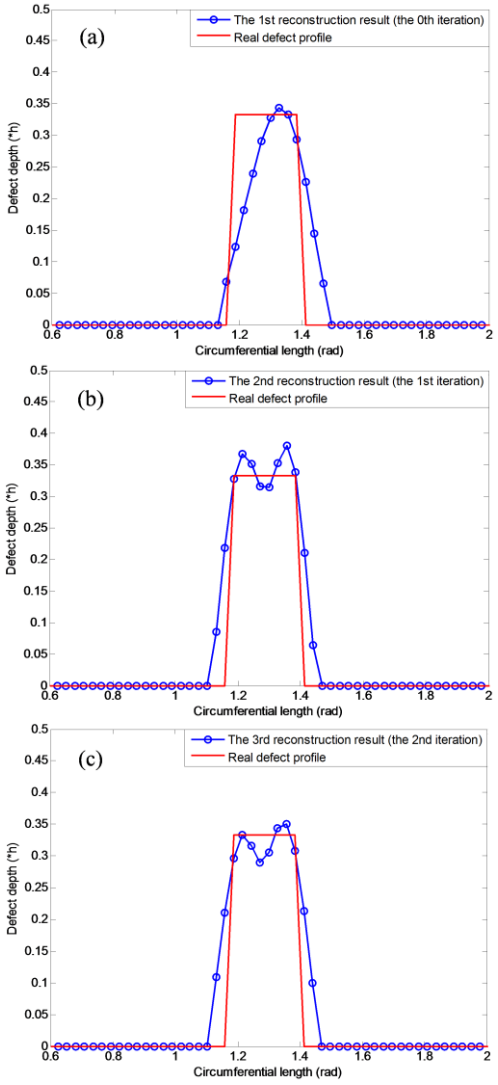

FIGURE 6. **Reconstruction results of rectangular defect by the iterative method: (a) the first reconstruction result; (b) the second reconstruction result; (c) the third reconstruction result.**

B. THREE TYPES OF DEFECTS

To further demonstrate the performance of QDFTU method for solving complex reconstruction problems, structures with different defects shown in Figs. 7, 9 and 11, are studied. Types of defects considered for reconstruction are: a multi-step flaw, a double-rectangular flaw, and a triple-rectangular flaw. Again, the initial reference model adopted is depicted in Fig. 4. To reconstruct a multi-step defect shown in Fig. 7, three iterations are required to obtain a converged result by applying the criterion defined in (14). The initial reconstruction is shown in Fig. 8(a), which can approximately identify the defect in the circumferential

extent and radial directions. After updating the reference model with initial reconstruction of the defect, the second reconstruction shown in Fig. 8(b) presents better circumferential and radial distributions, which reflects the main features of the multi-step defect. The third and fourth results in Fig. 8(c) and (d) depict more details of the defect, and the discrepancy of the fourth calculation ($\grave{o} = 0.026h$) also meets the RMSE criteria. Hence, the fourth result in Fig. 8(d) is deemed as the final solution to reconstruction of the multi-step defect.

The pipe structure with a double-rectangular defect in Fig. 9 is considered as a more complicated example to test the efficiency and accuracy of the developed QDFTU approach and the results are shown in Fig. 10. It is noted that the fluctuations in the first reconstruction (Fig. 10(a)) deteriorate the identification accuracy of the defect profile. This is because the integral coefficients $B_i(k)$ obtained from the reference model include redundant frequency components (or peak values), which was mentioned in Da et al.[28] Updating the reference model with the first result in the second reconstruction, the accuracy of the reconstructed defect profiles in Fig.10(b) is much improved. Due to the large difference between the first and second reconstruction results, the third reconstruction has to be performed. Since the discrepancy in the second iteration is less than the threshold value ($\grave{o} = 0.029h$), the final reconstruction of a double-rectangular defect shown in Fig. 10(c) is obtained.

In the fourth example, a triple-rectangular defect profile is described in Fig. 11. Employing the proposed QDFTU method, the reconstruction of such defect is achieved by updating the reference model three times. Defect profile after the initial reconstruction is given in Fig. 12(a). It is observed that the first reconstruction exhibits an acceptable agreement with the real defect profile. However, the gap length between two adjacent defects and the width of the defect cannot be predicted accurately. Similarly, to some extent the first and second updates of the reference model shown in Fig. 12(b and c) during the reconstruction process can improve the quality of defect detection, nevertheless, the defect depth by the reconstruction cannot be accurately obtained. Thus, the third update is activated and the defect profile is finally reconstructed with $\grave{o} = 0.028h$.

By comparisons of the first reconstruction and the last reconstruction results with the real defects in four numerical examples, the MSPE (mean absolute percentage error) values are shown in TABLE Ⅲ. Averagely, the accuracy of defect reconstruction results has been improved by the proposed method. The maximum enhancement of the precision for the multi-step defect problem is up to 17.18%, which is obtained from 30.93% in the first reconstruction to 13.75% in the last reconstruction; the minimum improvement in a triple-rectangular defect reconstruction example is 2.48%. Due to limitations from various sources on defect reconstruction, such as the initial reference model, the resolution of guided waves and the element size, it is difficult to obtain much improved results in all four examples. To further improve the accuracy of the reconstruction, future research on these factors is suggested.

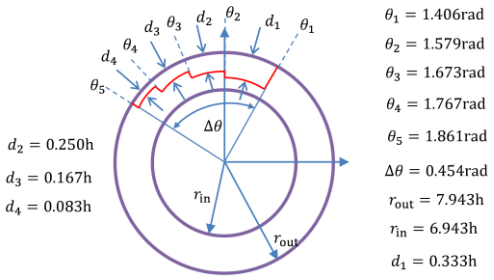

FIGURE 7. The tested model with a multi-steps defect. The area enclosed by the red lines represents defect.

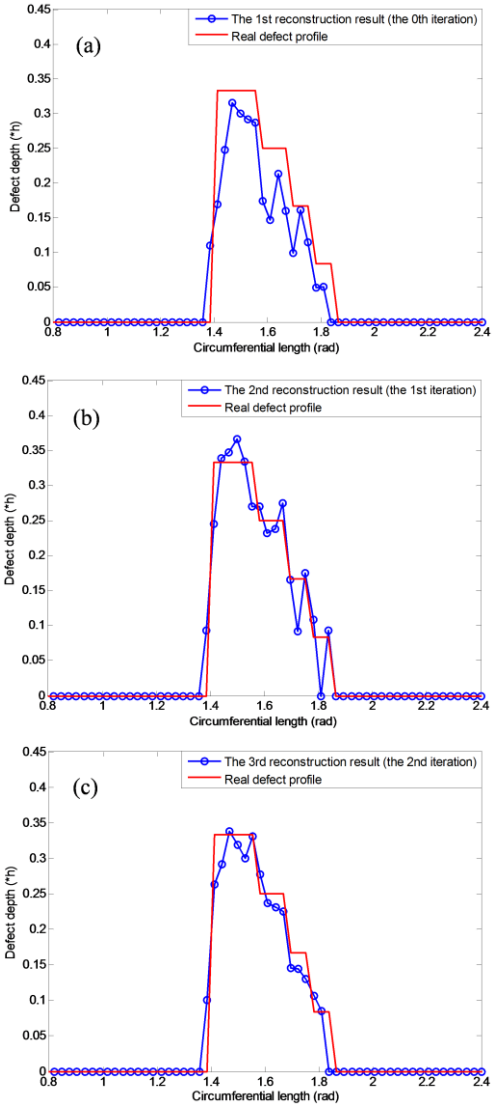

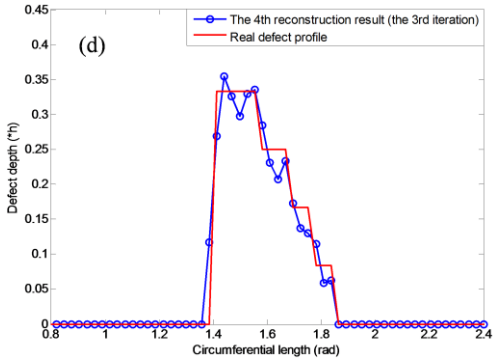

FIGURE 8. The reconstruction results of a multi-step defect by the iterative method: (a) the first reconstruction result; (b) the second reconstruction result; (c) the third reconstruction result; (d) the fourth reconstruction result.

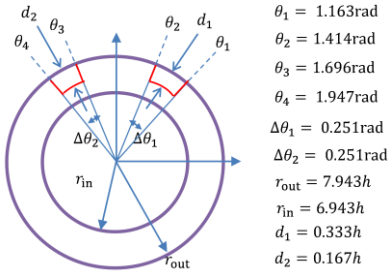

FIGURE 9. The tested model with a double-rectangular defect. The area enclosed by the red lines represents defect.

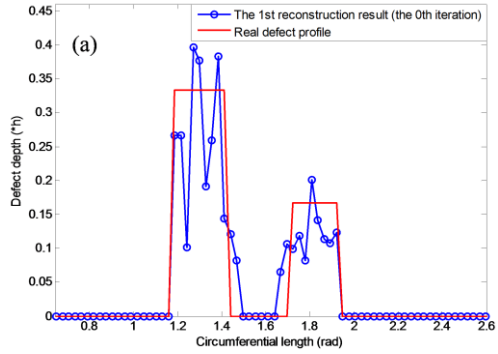

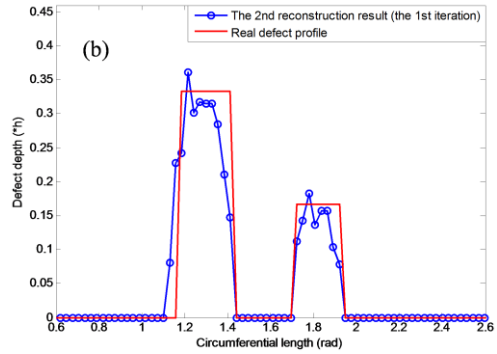

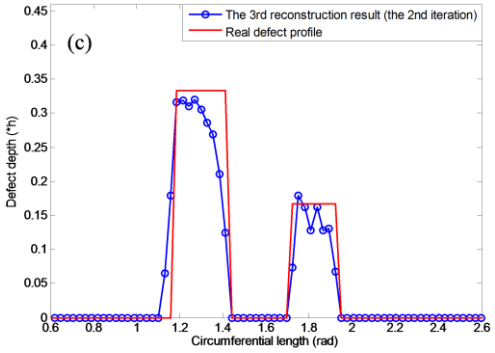

FIGURE 10. The reconstruction results of a double-rectangular defect by the iterative method: (a) the first reconstruction result; (b) the second reconstruction result; (c) the third reconstruction result.

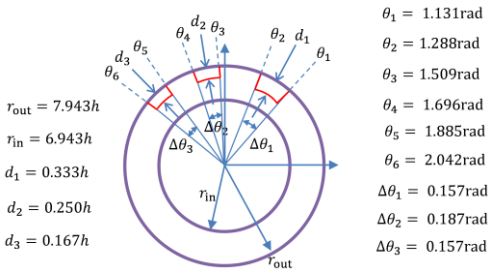

FIGURE 11. The tested model with a triple-rectangular defect. The area enclosed by the red lines represents defect.

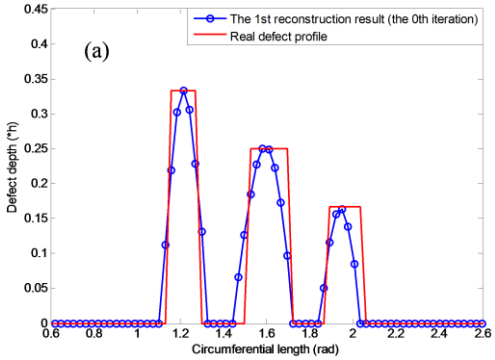

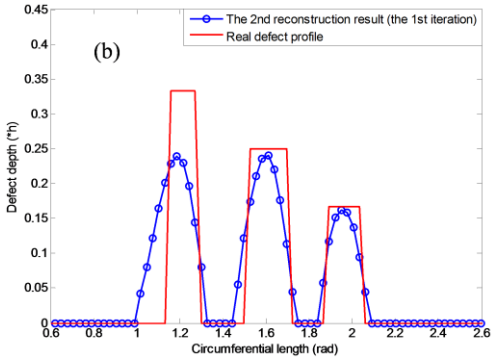

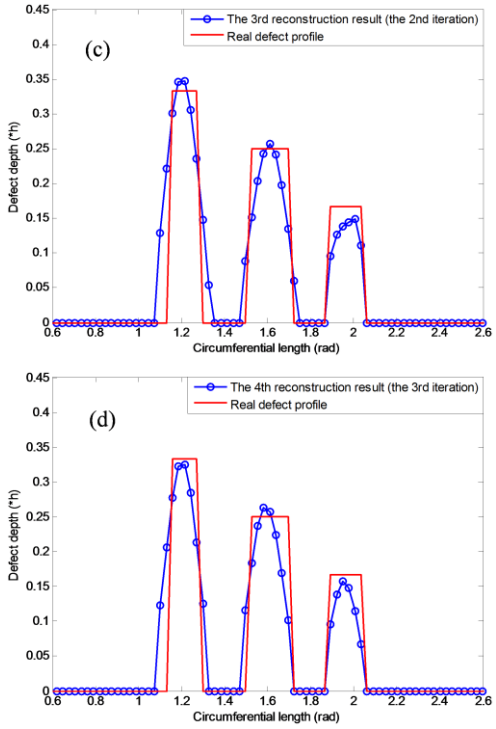

FIGURE 12. The reconstruction results of a triple-rectangular defect by the iterative method: (a) the first reconstruction result; (b) the second reconstruction result; (c) the third reconstruction result; (d) the fourth reconstruction result.

TABLE III
THE MSPE (MEAN ABSOLUTE PERCENTAGE ERROR) VALUES IN ALL FOUR EXAMPLES

MSPE	A single rectangular defect	A multi-step defect	A double-rectangular defect	A triple-rectangular defect
The first reconstruction	20.76%	30.93%	31.09%	23.77%
The last reconstruction	6.69%	13.75%	21.06%	21.29%

V. CONCLUSION

In this paper, a modified QDFT (Quantitative Detection of Fourier Transform) method with integration of an integral coefficient updating strategy (QDFTU) has been proposed to improve the defect detection precision. QDFTU overcomes the problem that the iteration reconstruction method cannot be introduced to the traditional boundary integral equation. And comparing other general methods, this investigation avoids the difficulty of solving the analytical fundamental solution in pipeline structure. Reconstructions of four types of defects in pipe structures have been examined. The entire reconstruction must include signal processing, reference model update, and convergence judgment so that the accurate and efficient defect detection can be conducted. To update the reference model by the proposed strategy, root mean square error measured by the difference between two consecutive reconstruction profiles is adopted as a convergence criterion. It is concluded that the more complex the defect is, the more the number of updates for reconstruction is required. In the detection of complex defected structures for example, pipes with a multi-step flaw or a triple-rectangular flaw, the proposed QDFTU approach outperforms QDFT in terms of predictions on the details, e.g., the step length, the gap length, and the defect extent. Although there is noise disturbance during the reconstruction of defects, the results converge after just three updates of the reference model. The maximum and minimum enhancements of the reconstruction precision is up to 17.18% for the multi-step defect example and 2.48% in the triple-rectangular defect case study, respectively. This proves the proposed QDFTU approach has ability to reconstruct defects with high levels of efficiency and accuracy. To further improve the reconstruction results, the increased resolution of guided waves and number of elements for the model are suggested. In conclusion, the proposed QDFTU can accurately and efficiently reconstruct complex defects using ultrasonic guided waves and provide insights into the mechanism of defect detections using a general reference model.

REFERENCES

[1] M. Kachanov, “Effective elastic properties of cracked solids: critical review of some basic concepts,” *Appl Mech Rev*, vol. 45, no. 8, pp. 305–336, 1992.

[2] M. Kachanov, I. Sevostianov, *Quantitative Characterization of Microstructures in the Context of Effective Properties*, In: Micromechanics of Materials, with Applications, Solid Mechanics and Its Applications. Springer, Cham, 2018, pp. 113–135.

[3] I. Sevostianov, S. G. Mogilevskaya, V. I. Kushch, “Maxwell's methodology of estimating effective properties: Alive and well,” *International Journal of Engineering Science*, vol. 140, pp. 35–88, 2019.

[4] K. R. Leonard, E.V. Malyarenko, M.K. Hinders, “Ultrasonic lamb wave tomography,” *Inverse Problems*, vol. 18, no. 6, pp. 1795–1808, 2002.

[5] P. Huthwaite, “Evaluation of inversion approaches for guided wave thickness mapping,” *Proceedings of the Royal Society A: Mathematical, Physical and Engineering Sciences*, vol. 470, no. 2166, pp. 20140063, 2014.

[6] P. Huthwaite, “Guided wave tomography with an improved scattering model,” *Proceedings. Mathematical, physical, and engineering sciences*, vol. 472, no. 2195, pp. 20160643, 2016.

[7] J. Rao, M. Ratassepp, Z. Fan, “Investigation of the reconstruction accuracy of guided wave tomography using full waveform inversion,” *Journal of Sound and Vibration*, vol. 400, pp. 317–328, 2017.

[8] N. Hosoya, A. Yoshinaga, A. Kanda, I. Kajiwara, “Non-contact and non-destructive Lamb wave generation using laser-induced plasma shock wave,” *International Journal of Mechanical Sciences*, vol. 140, pp. 486–492, 2018.

[9] A. V. Razgulin, N. G. Iroshnikov, A. V. Larichev, T. E. Romanenko, A. S. Goncharov, “Fourier domain iterative approach to optical sectioning of 3d translucent objects for ophthalmology purposes,” *The International Archives of Photogrammetry, Remote Sensing and Spatial Information Sciences*, vol. XLII-2/W4, pp. 173, 2017.

[10] S. Fan, S. Smith-Dryden, J. Zhao, S. Gausmann, A. Schulzgen, G. Li, B. Saleh, “Optical Fiber Refractive Index Profiling by Iterative Optical Diffraction

Tomography," *Journal of Lightwave Technology*, vol. 36, no. 24, pp. 5754–5763, 2018.

[11] E. J. Lee, K. H. Cho, K. B. Kim, S. R. Lim, T. Kim, J. Kang, B. Ju, S. Park, M. Park, D. Kim, "Optical Reconstruction of Full-color Optical Scanning Holography Images using an Iterative Direct Binary Search Algorithm," *Journal of the Korean Physical Society*, vol. 73, no. 12, pp. 1845–1848, 2018.

[12] K. M. S. Uddin, Q. Zhu, "Reducing image artifact in diffuse optical tomography by iterative perturbation correction based on multiwavelength measurements," *Journal of biomedical optics*, vol. 24, no. 5, pp. 1, 2019.

[13] Y. T. Solano-Correa, F. Bovolo, L. Bruzzone, "An approach to multiple change detection in vhr optical images based on iterative clustering and adaptive thresholding," *IEEE Geoscience and Remote Sensing Letters*, vol. 16, no. 8, pp. 1334–1338, 2019.

[14] K. Sauer, C. Bouman, "A local update strategy for iterative reconstruction from projections," IEEE Transactions on Signal Processing, vol. 41, no. 2, pp. 534–548, 1993.

[15] K. Wang, R. Su, A. A. Oraevsky, M. A. Anastasio, "Investigation of iterative image reconstruction in three-dimensional optoacoustic tomography," *Physics in Medicine and Biology*, vol. 57, no. 17, pp. 5399–5423, 2012.

[16] M. Beister, D. Kolditz, W. A.Kalender, "Iterative reconstruction methods in X-ray CT," *Physica Medica*, vol. 28, no. 2, pp. 94–108, 2012.

[17] P. Huthwaite, F. Simonetti, "High-resolution guided wave tomography," *Wave Motion*, vol. 50, no. 5, pp. 979–993, 2013.

[18] D. Yang, X. Shang, A. Malcolm, M. Fehler, H. Baek, "Image registration guided wavefield tomography for shear-wave velocity model building," Geophysics, vol. 80, no. 3, pp. U35–U46, 2015.

[19] J. Rao, M. Ratassepp, Z. Fan, "Guided wave tomography based on full waveform inversion," *IEEE transactions on ultrasonics, ferroelectrics, and frequency control*, vol. 63, no. 5, pp. 737–745, 2016.

[20] N. Nishimura, S. Kobayashi, "A boundary integral equation method for an inverse problem related to crack detection," *International Journal for Numerical Methods in Engineering*, vol. 32, no. 7, pp. 1371–1387, 1991.

[21] B. Wang, C. Yang, Z. Qian, "Forward and inverse analysis of love wave scattering by interface cavities," *Journal of Theoretical and Computational Acoustics*, vol. 27, no. 3, pp. 1850049, 2019.

[22] R. Chapko, D. Gintides, L. Mindrinos, "The inverse scattering problem by an elastic inclusion," *Advances in Computational Mathematics*, vol. 44, no. 2, pp. 453–476, 2018.

[23] M. Slaney, A. C. Kak, L. E. Larsen, "Limitations of Imaging with First-Order Diffraction Tomography," *IEEE Transactions on Microwave Theory and Techniques*, vol. 32, no. 8, pp. 860–874, 1984.

[24] M. Kitahara, K. Nakahata, S. Hirose, "Elastodynamic inversion for shape reconstruction and type classification of flaws," *Wave Motion*, vol. 36, no. 4, pp. 443–455, 2002.

[25] P. Belanger, P. Cawley, F. Simonetti, "Guided wave diffraction tomography within the born approximation," *IEEE Transactions on Ultrasonics, Ferroelectrics, and Frequency Control*, vol. 57, no. 6, pp. 1405–1418, 2010.

[26] L. J. Cunningham, A. J. Mulholland, K. M. M. Tant, A. Gachagan, G. Harvey, C. Bird, "A spectral method for sizing cracks using ultrasonic arrays," *Inverse Problems in Science and Engineering*, vol. 25, no. 12, pp. 1788–1806, 2017.

[27] B. Wang, Z. Qian, S. Hirose, "Inverse Shape Reconstruction of Inner Cavities Using Guided SH-Waves in a Plate," *Shock and Vibration*, vol. 2015, pp. 1–9, 2015.

[28] Y. Da, G. Dong, B. Wang, D. Liu, Z. Qian, "A novel approach to surface defect detection," *International Journal of Engineering Science*, vol. 133, pp. 181–195, 2018.

[29] R. Kazys, P. J. Mudge, R. Sanderson, C. Ennaceur, Y. Gharaibeh, L. Mazeika, A. Maciulevicius, "Development of ultrasonic guided wave techniques for examination of non-cylindrical components," *Physics Procedia*, vol. 3, pp. 833–838, 2010.

[30] W. Cailly, H. Walaszek, S. Brzuchacz, F. Zhang, P. Lasaygues, "Low-Frequency Guided Wave Quantitative Reconstruction of Corrosion in Plates, 1D Diffraction Problem," *ACTA ACUSTICA UNITED WITH ACUSTICA*, vol. 105, no. 6, pp. 970-986, 2019.

[31] J. He, D. C. Rocha, P. Sava, "Guided Wave Tomography Based on Least-Squares Reverse-Time Migration," *Structural Health Monitoring*, vol. 19, no. 4, pp. 1237-1249, 2020.

[32] X. Xining, Z. Lu, X. Bo, Y. Zujun, Z. Liqiang, "An Ultrasonic Guided Wave Mode Excitation Method in Rails," *IEEE Access*, vol. 6, pp. 60414-60428, 2018.

[33] X. Wei, Y. Yang, J. Ureña, J. Yan and H. Wang, "An Adaptive Peak Detection Method for Inspection of Breakages in Long Rails by Using Barker Coded UGW," *IEEE Access*, vol. 8, pp. 48529-48542, 2020.

[34] Y. Liu, Z. Li, K. Gong, "Detection of a radial crack in annular structures using guided circumferential waves and continuous wavelet transform," *Mechanical Systems and Signal Processing*, vol. 30, pp. 157–167, 2012.

[35] R. M. Sanderson, D. A. Hutchins, D. R. Billson, P. J. Mudge, "The investigation of guided wave propagation around a pipe bend using an analytical modeling approach," *Journal of the Acoustical Society of America*, vol. 133, no. 3, pp. 1404–1414, 2013.

[36] E. Leinov, M. J. S. Lowe, P. Cawley, "Investigation of guided wave propagation and attenuation in pipe buried in sand," *Journal of Sound and Vibration*, vol. 347, pp. 96–114, 2015.

[37] J. Qu, Y. Berthelot, Z. Li, "Dispersion of guided circumferential waves in circular annulus," *Review of Progress in Quantitative NDE*, vol. 15, pp. 169–176, 1996.

[38] G. Liu, J. Qu, "Guided circumferential waves in a circular annulus," *Journal of Applied Mechanics*, vol. 65, no. 2, pp. 424–430, 1998.

[39] C. Valle, M. Niethammer, J. Qu, L. J. Jacobs, "Crack Characterization using guided circumferential waves," *Journal of the Acoustical Society of America*, vol. 110, pp. 1282–1290, 2001.

[40] W. Luo, J. L. Rose, H. Kwun, "Circumferential shear horizontal wave axial-crack sizing in pipes," *Research in Nondestructive Evaluation*, vol. 15, pp. 149–171, 2004.

[41] S. Wang, S. Huang, W. Zhao, Z. Wei, "3D modeling of circumferential SH guided waves in pipeline for axial cracking detection in ILI tools," *Ultrasonics*, vol. 56, pp. 325–331, 2015.

[42] M. Clough, M. Fleming, S. Dixon, "Circumferential guided wave emat system for pipeline screening using shear horizontal ultrasound," *NDT & E International*, vol. 86, pp. 20–27, 2017.

[43] Y. Da, G. Dong, Y. Shang, B. Wang, D. Liu, Z. Qian, "Circumferential defect detection using ultrasonic guided waves: An efficient quantitative technique for pipeline inspection," *Engineering Computations*, vol. 37, no. 6, pp. 1923–1943, 2020.

[44] H. Zhang, Y. Du, J. Tang, G. Kang, H. Miao, "Circumferential SH wave piezoelectric transducer system for monitoring corrosion-like defect in large-diameter pipes," *Sensors (Basel, Switzerland)*, vol. 20, no. 2, pp. 460, 2020.

[45] S. V. Biryukov, Y. V. Gulyaev, V. V. Krylov, V. P. Plessky, *Surface Acoustic Waves in Inhomogeneous Media*. New York: Springer-Verlag, 1995, pp. 198–205.
[46] N. Rattanawangcharoen, A. H. Shah, S. K. Datta, "Wave propagation in laminated composite circular cylinders," *International Journal of Solids and Structures*, vol. 29, no. 6, pp. 767–781, 1992.
[47] W. Zhuang, A. H. Shah, "Elastodynamic Green's function for laminated anisotropic circular cylinders," *Journal of Applied Mechanics*, vol. 66, pp. 665–674, 1999.